



Mixed mode peeling of spinnable carbon nanotube webs



Noman Khandoker^{a,c,*}, Raafat Ibrahim^a, Wenyi Yan^a, Stephen C. Hawkins^{b,d}, Chi P. Huynh^c

^a Department of Mechanical and Aerospace Engineering, Monash University, Clayton, Victoria, Australia

^b School of Mechanical and Aerospace Engineering, Queen's University Belfast, United Kingdom

^c CSIRO Material Science and Engineering (CMSE), Bayview Avenue, Clayton, Victoria, Australia

^d Department of Materials Engineering, Monash University, Clayton, Victoria, Australia

ARTICLE INFO

Article history:

Received 27 February 2014

Accepted 30 April 2014

Available online 9 May 2014

Keywords:

Spinnable carbon nanotubes

Van der Waals energy

Cohesive law

Mixed mode fracture mechanics

ABSTRACT

This paper presents the study on interaction behaviour of spinnable carbon nanotubes by the peel test technique. Spinnable nanotube webs are used as macro scale experimental specimens to determine the mixed mode interaction behaviour between them. Numerical simulations are conducted to determine and compare the interfacial fracture energy of the interfaces in different orientations peeled at the same peel angle. The numerical model simulates the Van der Waals energy between nanotube webs through implementation of a cohesive law. The peeling process is simulated by considering a failure criterion based on continuum damage mechanics. It is shown that the interfacial energy varied with the orientation angle and the peel angle. Interfacial energy for parallel nanotube configuration is much higher than the crossed nanotube configuration. Increase in peel angle reduces the phase angle magnitudes so that the loading condition transforms from mode – II to mode – I resulting into reduction of the forces required to detach spinnable nanotubes. Hence, this study explores the spinnable nanotube interaction mechanics through which slippage may easily occur among them. Thus, the reason behind nanotube yarn failure before reaching large macroscopic stresses is better understood even though individual spinnable nanotube found to be very strong.

© 2014 Elsevier Ltd. All rights reserved.

1. Introduction

Carbon nanotubes (CNTs) are the prominent example of carbon nano materials. Existence of CNTs may be traced back to nearly two centuries ago but they were first reported in early 1950s [1,2]. However, report by Iijima and Ichihashi [3] drew attention of broader scientific community on CNT and triggered the massive research interests. Individual CNT is like a hollow cylinder invisible to naked eye. Trillions of these invisible cylinders need to be assembled to make useful macroscopic item. Carbon nanotube sheet known as web may become such a useful article. A CNT web is highly oriented and a free standing construct of spinnable CNTs. The nanotube webs are drawn from a side wall of draw able nanotube forests which are grown on a silicon wafer by chemical vapour decomposition (CVD) process. The key parameters for being a nanotube forest to be draw able are the alignment of the nanotube bundles and their entangled interconnections [4]. These entangled interconnections peel off the nanotube bundles from

the nanotube forest to form the web. Carbon nanotubes in the web settle together in a random network of free standing form due to the interactions among them caused by the Van der Waals attractive force. Nanotube web can then be twisted and spun into nanotube yarn. The strength of individual spinnable carbon nanotube is very high [5]. However, neither pure bulk nor composite applications, aimed at exploiting its strength, have succeeded in demonstrating this potential at a macroscopic scale. The reasons for this may lie in the mechanism in which real individual CNTs interact with each other. Thus nanotube interaction plays a key role in mechanical performance of macroscopic nanotube item. Quantitative experimental evaluation of nanotube interaction behaviour is very limited in current literature, which is quite obvious due to technical challenges associated with the nano scale mechanical manipulation of nano structures. In spite of technical challenges the measured Van der Waals force among single MWNT shells is 9 nN [6] and shear force between two MWNTs outer shells is 15–50 nN [7]. However, the orientation direction of nanotubes in these experiments is only along the length of the cylindrical axis. The effect of orientation angles between the cylindrical axis of two nanotubes could not be experimentally realised. Therefore, one of the objectives of this paper is to identify the relationship between Van der Waals energy and the orientation angle of

* Corresponding author at: Department of Mechanical and Aerospace Engineering, Monash University, Clayton, Victoria, Australia. Tel.: +61 3 99051088.

E-mail addresses: khandoker.noman@monash.edu, kna.noman@gmail.com (N. Khandoker).

spinnable nanotubes by numerical simulation. A theoretical investigation [8] showed the interaction between two single walled nanotubes crossed at an angle, which is used to verify our results. Peeling is the functional technique of nanotube detachment from its forest. Hence, peel test is employed to study nanotube interaction.

The peel test has been widely used to test the bonding strength of adhesives. Nowadays it is being used in many different forms and mechanisms in various fields of applications [9,10]. In this test a thin adherent attached to a substrate by adhesives is pulled at a certain angle known as peel angle and peeling force required to produce debonding is measured. In this test configuration the interface between the adherent and the substrate is subjected to both the normal and shear forces. Therefore, the debonding occurs in mixed mode interfacial fracture. There are several elastic analyses of peel test available in the early literatures on the subject [11–13]. They have represented the adherent and the substrate as an elastic beam on an elastic foundation. Simple energy balance procedure was used to calculate the debonding surface energy. Finite element analysis has also been used to study the interfacial stress distribution of the bond [14]. Initially the debonding of the joint was looked as a phenomenon of stress based failure criterion. However, experiments have shown that the energy release rate controls the debonding propagation. Hence, the use of total energy balance approach to determine the interfacial fracture strength is more appropriate than the stress based approach. To establish consistent results between the energy based approach and the stress based approach, large displacement analysis of the debonded peel arm was introduced by Gent and Hamed [15]. Thereafter, the energy based approach became fully established including calculation of the plastic energy dissipation due to bent radius and due to root rotation phenomena [16,17].

Linear elastic and nonlinear fracture mechanics approach was also used to study the mechanics of peel test. The notable aspect of fracture mechanics approach is that the fracture energy is independent of test specimen dimensions and features such as peel angle. Commonly large peel angles are used for such analysis which implicates existence of mode – I only. The issue of mode mixity in peel mechanics is addressed by Thouless and Jensen [18] utilising the interfacial crack analysis theory developed by Suo and Hutchinson [19]. They showed that in absence of adherent and substrate modulus mismatch the mode mixity is essentially constant with the peel angle. Consequently, their following parametric study of the peel test [20] ignores the effect of mode mixity on interface fracture. However, the role of mode mixity may be of crucial importance. As mentioned earlier, spinnable nanotubes peel from bundles of nanotubes in the CVD grown forests to form the nanotube web. The entire process of nanotube web formation is very complex. But the entire process is initiated and dependent on peeling mechanism of nanotubes [4]. Thus far understanding the peeling mechanism in carbon nanotube interaction is limited only in qualitative discussions with the peel angle. To fully realise the interaction process mix mode factor of the peel mechanics need to be quantitatively investigated and thus identify the range of peel angle where it plays a crucial role.

This paper analyses the interface between webs of spinnable carbon nanotubes. The main application towards which this study is directed is the case of interaction behaviour of spinnable carbon nanotubes. The aim is to establish an experimentally validated benchmark model of the interface which will help to study their interaction behaviour at different orientation directions. Thus the main objective of this research is to compute the debonding load and to evaluate the interfacial fracture energy for different orientation angles of spinnable nanotubes. The peel mechanism as a function of peel angle is also simulated and studied based on linear elastic fracture mechanics principles combined with damage based

failure analysis. Thus the effect of mode mixity on the interfacial strength can be thoroughly evaluated. The developed numerical model in this research is validated by experimental results. The experiments were performed with macro level carbon nanotube construct; i.e. nanotube webs. The ultimate goal of this research is to evaluate the peeling mechanism in terms of peeling angle and orientation angle of spinnable nanotubes so that interactions of nanotubes can be better understood.

2. Experimental setup

2.1. Sample preparation

The carbon nanotube webs used in this study is prepared from spinnable MWNTs grown as a forest on silicon wafer by chemical vapour decomposition (CVD) process. This used semiconductor grade Si substrates, with a thermal oxide layer of 50 nm thick and an iron catalyst coating of 2.5 nm deposited by e-beam evaporation. A 44 mm inner diameter quartz reactor was fed with an acetylene concentration of 2.4% in helium (25 sccm in 1000 sccm He) with a running time of 10 min and temperature of 680 °C. More details of this process are published elsewhere [21]. The vertically aligned MWNTs in the forest can be drawn into a web of CNTs which is the major assessment indicator for the spinnability property of carbon nanotubes [22]. The web was initiated with the sharp edge of a scalpel plunged down into the forest and then by pulling it away perpendicular to the nanotube growth direction. The CNTs from the forest string out behind the scalpel and hold together without any presence of binding agent.

The peel test samples were prepared as symmetrical test specimens by laying CNT webs on an alumina block. Layers of the webs are shown in Fig. 1. Before lay up of webs the alumina block was cleaned and rinsed with hot water and oven dried at 350 °C for 30 min. After cooling down to room temperature the block was attached to the web winding apparatus by double sided Kapton tape. The web winding apparatus consists of a DC motor and a spindle with winding mechanism specially designed and set up in house for winding spinnable CNT webs. Ten layers of webs were put on the block for the bottom part without any pressure applied on them. The bottom part web is then densified with drops of acetone. Later on a polymer sheet was laid on top of the bottom part at one side of the block which acts as a separator between the top part and the bottom part of the webs. The block was then detached and manually repositioned on the apparatus, suitable approximately for the preferred average orientation angle of the top part. Subsequently ten CNT web layers for the top part were laid without any pressure applied on them and densified with drops of acetone. Very low concentration of acetone was used for the purpose of densification to avoid contamination. Sample specimens were then rest apart for the evaporation of acetone. Spinnable nanotubes tend to stick to each other when they are in contact. Therefore, as the layers are laid nanotube webs are adhered together. The volumetric density of as produced single layer of web is 0.0015 g/cm³. The densification process increases this single layer density to 0.5 g/cm³ [23]. The evaporation of acetone during densification process causes surface tension affecting shrinkage on each of the web layer thickness to 50 nm. Thus density of web is increased and contact is established between the top and bottom adherents except where the polymer separator is placed. As the densified web is a porous material, the contact between these two surfaces is discrete point to point contact in nature. The samples were inspected under digital microscope camera and measurements were taken for the orientation angle, width and effective overlap length of the specimens. Three specimens were tested for each cross angled interface of carbon nanotubes.

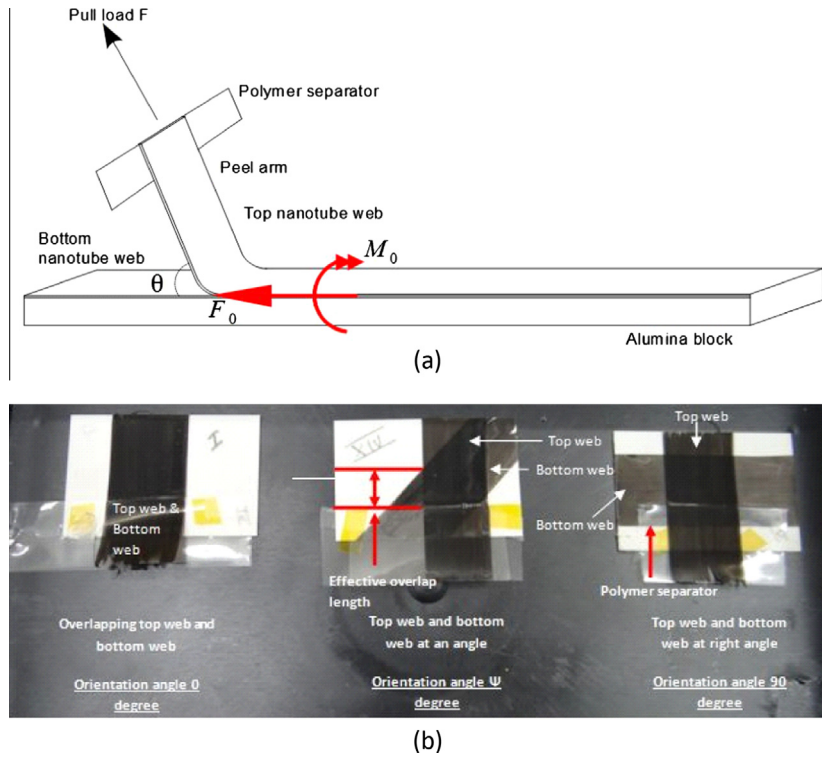


Fig. 1. Symmetric peel test specimen. (a) Schematic 3D view of peel test specimen. (b) Peel test specimens.

2.2. Experimental procedure

The peeling experiments were conducted on an Instron tensile testing machine with a static load cell of 2.5 N capacities. These tests were quasi static in nature. Therefore, 2 mm/min load rate was applied in the tests. The specimen was placed on a flat surface and the peel arm was attached to the cross head of the Instron machine. Displacement control method was used to apply the load on the specimen. The load displacement response from the test was recorded automatically to the computer interfaced to the Instron machine. The video of whole test was digitally recorded with bookmarks for the debonding of the effective overlap section of the specimens. The test was manually stopped as soon as the cross head displacement caused the interface to debond up to the effective overlap length. Later the video was synchronised with the recorded load displacement data and image frames were extracted to be processed for the peel angle data.

3. Numerical modelling of peel test

3.1. Problem definition

The physical problem of a peel test can be treated as either a plane stress or a plain strain problem as shown in Fig. 1. In a peel test peeling force is applied uniformly in normal direction of the cross section at one edge of the top adherent. In this investigation a quasi static peel process is assumed which corresponds to the cases of low peeling rates. The top and bottom adherents nanotube web are extremely flexible. Therefore, the plastic deformation is not considered in this paper. The top and bottom adherends is modelled in this paper as anisotropic materials. The exact anisotropic characteristics of nanotube webs are not available from any theoretical or experimental studies. Therefore, the closest possible match for the material properties is used. The following anisotropic constitutive relationship of graphite is used for this purpose [24].

$$\begin{Bmatrix} \sigma_x \\ \sigma_y \\ \sigma_z \\ \tau_{yz} \\ \tau_{zx} \\ \tau_{xy} \end{Bmatrix} = \begin{bmatrix} 1060 & 180 & 15 & 0 & 0 & 0 \\ 180 & 1060 & 15 & 0 & 0 & 0 \\ 15 & 15 & 36.5 & 0 & 0 & 0 \\ 0 & 0 & 0 & 4.5 & 0 & 0 \\ 0 & 0 & 0 & 0 & 4.5 & 0 \\ 0 & 0 & 0 & 0 & 0 & 440 \end{bmatrix} \begin{Bmatrix} \epsilon_x \\ \epsilon_y \\ \epsilon_z \\ \gamma_{yz} \\ \gamma_{zx} \\ \gamma_{xy} \end{Bmatrix} \quad (1)$$

The unit of modulus is in GPa. The commercial finite element code Abaqus was used to investigate the peel mechanics. The simulation was set up in two dimensional plane strain model setting. The bottom of the model is constrained in all degrees of freedom. The model contains four node reduced integration plane strain elements of size $0.05 \times 500 \mu\text{m}$. The interface between the top and bottom adherents is modelled by contact definition with cohesive zones. Due to contact definition the adherents do not penetrate each other even if small peel angle is used in the simulation.

3.2. Cohesive zone law

Cohesive zone law establishes the traction-separation relationship for the interface. In this paper, bilinear uncoupled cohesive laws of wide applicability [25] are considered both in normal and shear directions as illustrated in Fig. 2. The traction across the interface increases and reaches a peak value, then decreases and eventually vanishes, permitting a complete decohesion. The traction separation model follows a linear elastic behaviour followed by the initiation and evolution of damage. The elastic behaviour is defined in terms of an elastic constitutive matrix that relates the nominal stresses to the nominal strains across the interface as follows.

$$P = \begin{Bmatrix} P_n \\ P_s \\ P_t \end{Bmatrix} = \begin{bmatrix} K_{nn} & & \\ & K_{ss} & \\ & & K_{tt} \end{bmatrix} \begin{Bmatrix} \epsilon_n \\ \epsilon_s \\ \epsilon_t \end{Bmatrix} = K \epsilon \quad (2)$$

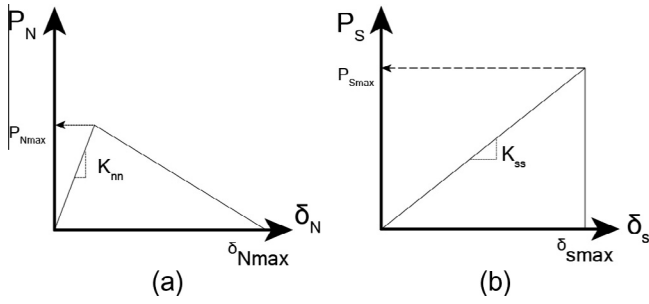


Fig. 2. Interfacial cohesive law (a) Normal direction (b) Shear direction.

P_{Nmax} and P_{Smax} are the damage initiation condition under the mixed mode loading of the peel test. Once the failure criterion is met in the cohesive zone the contact definition does not exist anymore to that particular location. Correlating to energy-based fracture mechanics, the fracture energy G_{Jf} and G_{IIJf} , i.e., the pure mode I and mode II fracture energy, is the area under the force–displacement curve illustrated in Fig. 2, which can be calculated as

$$\begin{aligned} G_{Jf} &= \frac{1}{2} P_{Nmax} \delta_{Nmax} \\ G_{IIJf} &= \frac{1}{2} P_{Smax} \delta_{Smax} \end{aligned} \quad (3)$$

4. Experimental results and discussion

During the progress of the peel tests the failure types of the specimens were observed. The debonding was initiated through the polymer separator between the adhered nanotubes webs. In all of the tests the interface debonded along the bond line leaving the top and bottom adhered intact. Therefore, the interface failure occurred in all of these peel tests were cohesive in nature.

The experimental force displacement data points constitute the peel curve. The average peel curves obtained for different orientation angles are presented in Fig. 3. The features of the peel curves are identified by two stages namely the initial peel stage and the steady state peel stage. The initial peel stage of the peel curves are considered to be within the first 20% of the applied extension. During this stage the interface crack front is established with elastic tensions acting in the adhered parts. As the force value increased linearly in this stage, it can be deduced that the peel system behaved elastically without any debonding extension. The

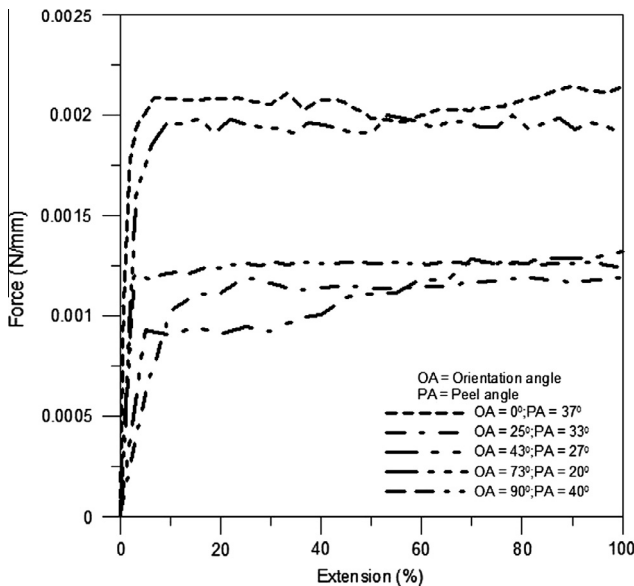


Fig. 3. Average experimental peel curves for different orientation angles.

steady state peel stage is reached when the peel curve attained a load plateau level at constant displacement. The debonding of the interface takes place during this steady state stage which is independent of the length of debond. The steady state peel force data is given in Table 1.

These peel curves are quiet similar in features but differ only in their steady state magnitudes. The interfacial energy can be directly calculated from these peel forces [12]. However, for different peel angles the effect of orientation angle on interfacial energy cannot be realised as the peel is inversely proportional to the peel angle for a specific nanotube orientation. With the aid of simulation we can rule out this factor when comparing the peel forces and thus interfacial energies for different orientation angles. This is presented in the next sections.

This interface energy calculated by peel force [12] includes energies dissipated due to all modes of mechanical deformations. To deduce the true interface fracture energy, corrections may be needed according to the peel deformation pattern [16]. These corrections are as follows.

- I. Energy dissipated due to tensile deformation in the peeling arm.
- II. Energy dissipated due to bending deformation of the peel arm.
- III. Energy dissipated due to root rotation at the peel front.

For anisotropic material the volumetric strain energy density in tension is

$$U = \frac{1}{2} S_{ijkl} \sigma_{ij} \sigma_{kl} \quad (4)$$

where S_{ijkl} is the elastic compliance tensor of the material and is σ the stress tensors. The magnitude of the stress tensors in this case should be considerably small as the applied force (Fig. 3) is very low. Therefore, the energy dissipated due to tensile deformation can be neglected. The bent radius should be taken into account when considering energy dissipation due to bending. Practically in the experiment the bent radius is much higher than the diameter of the constituent CNTs of the web. Therefore, the CNTs in the bend confront tensile mode of deformation rather than bending deformation. The root rotation phenomenon which can be modelled as two dimensional elastic beam on an elastic foundation with thickness of 50% beam height, expresses the fact that the beam does not act as a truly built in beam. It extends in length by a factor known as its characteristic length. Williams et al. [26] deduced the expression of characteristic length for anisotropic material as follows.

$$\Delta = h \cdot \sqrt[4]{\frac{1}{6} \frac{E_1}{E_2}} \quad (5)$$

where h is the beam height and E_1 and E_2 are the modulus of elasticity of the beam's anisotropic material in two mutually orthogonal directions. Carbon nanotube webs are anisotropic in nature and the beam height in this equation is comparable with the thickness of the webs which is 500 nm in this study. Therefore, the magnitude for the characteristic length is extremely low. Therefore, energy dissipated for the root rotation is not considered in the present study. Hence, the energy obtained from Eq. (7) is directly considered as the interface fracture energy. This is further discussed in the following sections.

5. Numerical results and discussions

5.1. Numerical model validation

The numerical simulation model of the peel test is validated with the experimental results. For this purpose the force

Table 1
Peel test results for carbon nanotube webs at different orientation angles.

Experiment			Simulation
Average orientation angle (°)	Peel angle (°)	Peel force (nN/μm)	Peel force (nN/μm)
0	37 ± 4	1988 ± 89	2080
24	33 ± 4	1151 ± 205	1100
43	27 ± 4	966 ± 88	1000
73	20 ± 3	1940 ± 193	1948
90	40 ± 7	1200 ± 100	1218

displacement plots from experiments and from simulations are compared. In the simulations the peeling conditions were given as the data in Table 1. A comparative plot is shown in Fig. 4. It is to be noted here that as exact anisotropic material property for nanotube webs was unavailable it could not be used in these simulations. However, the level of attained steady state force matches closely with the experimental results. Thus, the simulated nanotube web interface is validated.

5.2. Interfacial energy

Interfacial energy of the nanotube web interface for different orientation angle can be obtained from the 90° peel simulations. The interfacial energy can be calculated from the analysis of peel test in terms of energy principles of Linear Elastic Fracture Mechanics (LEFM) theory. The debonding of the interface between the nanotube webs initiates when work done in breaking is exactly compensated by the gain in surface energy of the system. If U_T is the total energy and a is the crack length, then the interfacial fracture will occur if

$$\frac{dU_T}{da} = 0 \tag{6}$$

Using this criterion Kendall [12] deduced the interface energy G between the top and bottom adherents in a peel test as follows.

$$G = F(1 - \cos \theta) \tag{7}$$

where F is the peel force per unit width of the sample and θ is the peel angle. Thus for a 90° peel test the interface energy is the steady state force level attained from the simulation.

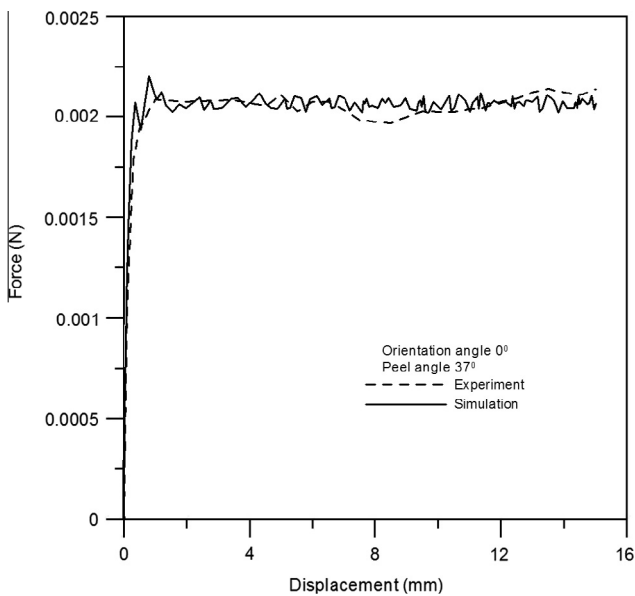


Fig. 4. Force displacement plots of peel test and simulation at 0° orientation angle.

The interface energy for different orientation angles are given in Fig. 5. The energy varies according to different cohesive parameters used in modelling the interface for different orientation angles. These cohesive parameters were chosen to match the simulation results with the average experimental peel curves presented in Fig. 3. Practically in absence of any binding agents the interface between CNT webs is originated from Van der Waals interactions between carbon nanotubes. Therefore, the force recorded in peel curves are the resultant reaction forces against the VDW forces between CNT webs. Van der Waals force is generated by instantaneous polarisation of atoms and molecules caused by quantum mechanical effect [27]. By using interaction potential w which is a function of separation distance s between the particles, the Van der Waals force f can be calculated for a pair of atoms or small molecules as follows.

$$w(s) = -\frac{C}{s^6} \tag{8}$$

$$f = -\nabla w \tag{9}$$

where C is material dependent interaction constant. The negative sign signifies the attractive nature of the force. The total Van der Waals force between macroscopic bodies can be derived from Eq. (9) considering the total volumes of bodies as follows.

$$F_{vdw} = -\rho_1 \rho_2 \int_{V_1} \int_{V_2} \nabla w dV_1 dV_2 \tag{10}$$

where ρ_i and V_i represent the number density and volume of body $i = 1, 2$. Eq. (10) does not have an analytical solution except in few special cases. Therefore, the integral has to be evaluated by numerical procedure. To reduce the computational complexity the volume integrals can be converted to surface integrals [28] by using the divergence theorem and assuming a vector field J such that

$$\nabla \cdot J = -w \tag{11}$$

By combining Eqs. (10) and (11) the following surface formulation of the total van der waals force is obtained.

$$F_{vdw} = \rho_1 \rho_2 \int_{S_1} \int_{S_2} (J \cdot n_1) \cdot n_2 dS_1 dS_2 \tag{12}$$

where ρ_i, S_i, n_i represent the atomic number density, boundary surface and outward pointing unit normal of surface $i = 1, 2$

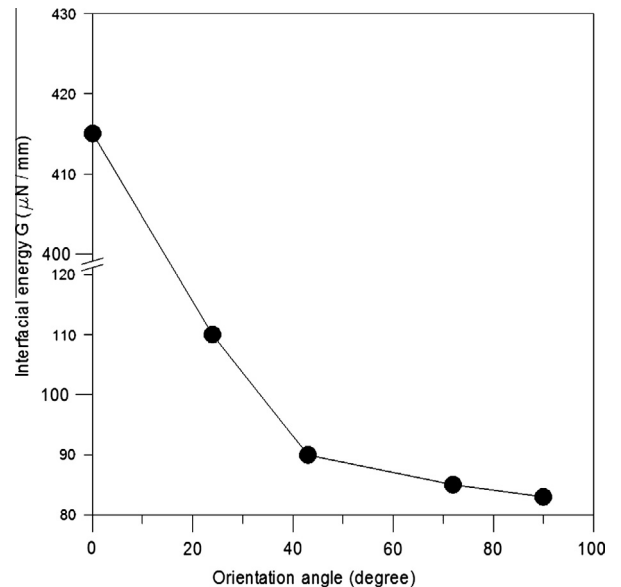


Fig. 5. Interfacial energy calculated from finite element simulations of peeling at 90° for different orientation angles of carbon nanotube webs.

respectively. If x is a vector from a point on body 2 to a point on body 1, then the distance s between these points become $s = (x \cdot x)^{1/2}$ and the expression for function J from Eq. (11) becomes as follows.

$$J = \frac{C \cdot x}{3(x \cdot x)^3} \quad (13)$$

The integration in Eq. (12) goes over all points on each surface. The orientation angle of the peel test geometry used in this study controls the magnitude of the vector x in Eq. (13). Thus if x is lower then J is higher and vice versa is applicable. When J is high magnitude of total VWD force become higher and vice versa is applicable. In case of parallel nanotubes x is lower but for crossed nanotubes x is higher. Thus peel force for zero degree orientation is highest and for other orientation angles decreases accordingly. Hence, the interfacial energy values differ in magnitudes for different orientation angles.

The nature of the peel energy of CNT webs is very complicated due to the anisotropy imposed by the hierarchical structure of web layout at different orientation angles. For simplification and ease of understanding, let us consider the interaction between a pair of nanotubes at different orientation angles. Using smeared out approximation Pogorelov et al. [8] deduced the expression for VDW energy (unit $eV \cdot A^2$) of crossed nanotubes at an angle as follows.

$$\phi(t_1, t_2, d) = \frac{v^2 \pi^2 \sqrt{t_1 t_2}}{d^3 \sin \gamma} \left[-A \left(\frac{1}{3} + \frac{\alpha d}{48} \right) + \frac{2B}{45d^6} \right] \quad (14)$$

In this equation d is the vertical distance between nanotubes, γ is the orientation angle, v is mean surface density of carbon atoms on the outer most shell of nanotube (unit A^{-2}), A is the attractive constant of Lennard Jones potential ($15.2eV \cdot A^6$), B is the repulsive constant of Lennard Jones potential ($24100eV \cdot A^{12}$) and $\alpha = 1/t_1 + 1/t_2$ and t_1, t_2 are the radius of the nanotubes. Let us consider the case for two crossed nanotubes with equal diameters and finite lengths along with other equal parameters resting at a distance $d \rightarrow 0$. Then the energy between these two nanotubes will inversely vary with respect to their orientation angle γ . However, this expression becomes singular for the parallel orientation at $\gamma = 0$. From Fig. 5 it can be seen that the energy in 0 degree orientation is comparably very high than other orientation angles. Moreover, the decreasing trend can also be seen along with the lowest level at 90° orientation. Thus the simulation results are also verified by the analytical approximation.

5.3. Mixed mode effect

The effect of mixed mode on peeling force can be studied by simulating the peeling action in different peel directions. For this purpose the 90° orientation angle interface is chosen. The force displacement plot for different peel angle is presented in Fig. 6. From this plot we can see that the steady state peel force decreases with the increase of the peel angle. This happens because of mode mixity nature of loading in higher peel angle. In mixed mode fracture mechanics analysis the degree of mode mixity is expressed by means of phase angle which is defined as follows.

$$\psi = \tan^{-1} \sqrt{\frac{G_{II}}{G_I}} \quad (15)$$

where G_I and G_{II} are mode – I and mode – II components of energy release rate respectively. The total energy release rate thus can be given by

$$G = G_I + G_{II} \quad (16)$$

For the peel test geometry Thouless and Jensen [18] expressed the mode – I and mode – II energy as follows.

$$G_I = \frac{6M_0^2}{Et^3} \quad G_{II} = \frac{F_0^2}{2Et} \quad (17)$$

$$F_0 = F \cos \theta \quad M_0 = \sqrt{\frac{Et^3}{6} \left[\frac{F^2 \sin^2 \theta}{2Et} + F(1 - \cos \theta) \right]} \quad (18)$$

where F_0 and M_0 are shown in Fig. 1. E and t are the modulus of elasticity and thickness of the adherent CNT web whose values for carbon nanotube web can be found from the article by Zhang et al. [23]. In peel test geometry interfacial fracture can be assumed to propagate when the total energy release rate G is equal to the mode dependent work of separation energy G_f which depends on the mixed mode fracture criterion. Laura De Lorenzis and G. Zavarise [29] proposed the following energy based mixed mode fracture criterion for peel test.

$$\frac{G_I}{G_{If}} + \frac{G_{II}}{G_{IIf}} = 1 \quad (19)$$

where G_{If} and G_{IIf} denote the fracture energies in pure mode – I and pure mode – II conditions respectively and can be determined experimentally [30]. Now by combining Eq. 15, 16, and 19 the following expression for $G_f(\psi)$ can be obtained [20].

$$G_f(\psi) = \frac{rG_{If}(1 + \tan^2 \psi)}{r + \tan^2 \psi} \quad (20)$$

where,

$$r = \frac{G_{IIf}}{G_{If}} \quad (21)$$

Assuming extensible adherents Williams [17] had also expressed the steady state energy release rate for a peel test as follows.

$$G = F \left(1 - \cos \theta + \frac{F}{2Et} \right) \quad (22)$$

Combining Eq. (20) and (22) and dividing by G_{If} the following dimensionless expression for the peel force can be obtained.

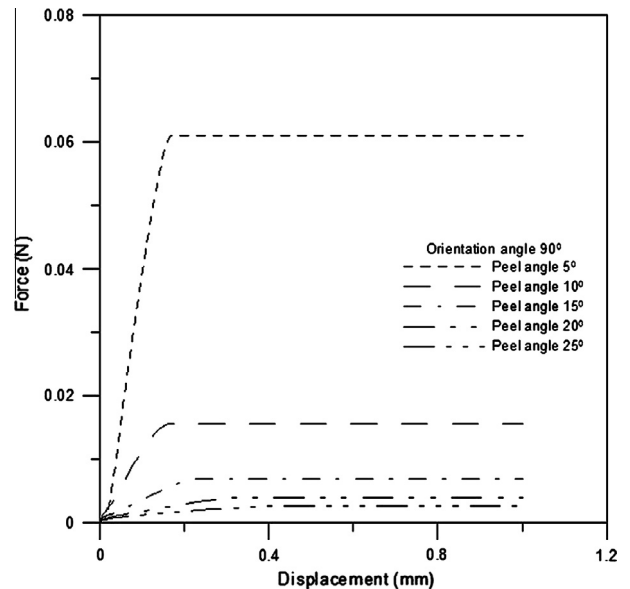


Fig. 6. Effect of peel angle on peel force for carbon nanotubes web at 90° orientation angle.

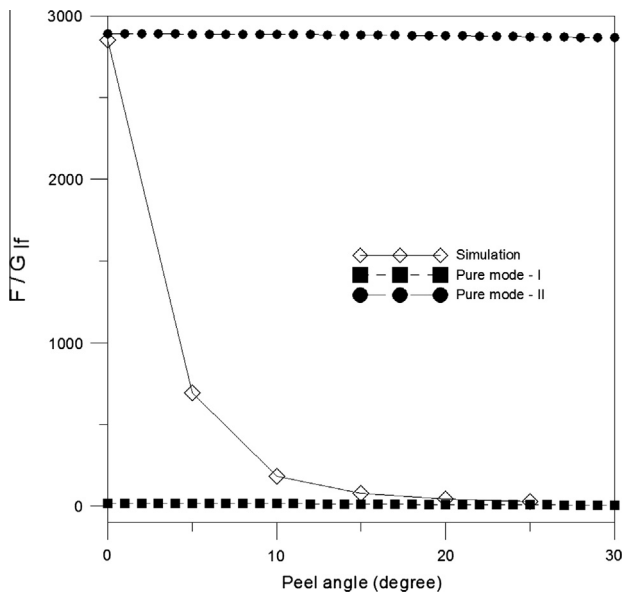


Fig. 7. Effect of mixed mode on peeling force for carbon nanotubes web at 90° orientation angle.

$$\frac{F}{G_{if}} = \sqrt{\left(\frac{Et}{G_{if}}\right)^2 (1 - \cos \theta)^2 + 2\frac{Et}{G_{if}} \frac{G_f(\psi)}{G_{if}} - \frac{Et}{G_{if}} (1 - \cos \theta)} \quad (23)$$

This expression shows the relationship of mode mixity with the peel angle. From analytical point of view if we take $G_f(\psi) = G_{if}$ then we obtain the pure mode – I status of peel force. Whereas, if we take $G_f(\psi) = G_{iff}$ then we obtain pure mode – II status of peel force. The pure mode – I and pure mode – II along with mixed mode data points from simulation is presented in Fig. 7. It can be seen that as the peel angle increased the peel force transforms from pure mode – II to pure mode – I due to decrease in phase angle magnitudes which can be calculated from Eq. (15). That is why the steady state peel force in Fig. 6 decreased with the increment of peel angle. The normalised peel force in Fig. 7 behaves asymptotically in mode – I as the peel angle increases. Therefore, mode mixity plays a crucial role in transforming fracture mode approximately within the peel angle of 0–20°. This interface mechanics is also observed in interfacial fracture toughness determination of coatings using circumferentially notched tensile specimens [31,32].

6. Conclusions

This paper presented the peeling mechanics of carbon nanotube webs. The effects of variations in peel angles and orientation angles between nanotubes on peel mechanics were revealed. Interfacial fracture energy, which originated from Van der Waals interactions in absence of any binding agent between the webs, decreased with the increment of the orientation angle. Therefore, the interface is very weak when the orientation angle between nanotubes is ninety degrees. However, it still possesses comparatively higher strength when they are aligned in parallel to each other at zero degree. Hence, the carbon nanotubes oriented in a parallel direction inside the nanotube yarn assists in bearing higher macroscopic stresses.

As for the peel angle, steady state peel force decreases with the increase in peel angle. This is because the mode – II loading condition at lower peel angles transforms into mode – I loading condition at higher peel angles due to the decrease in the phase angle of the loading condition. Nanotube bundles in the forest are mostly parallel to each other. The interconnections between these parallel nanotubes are connected at different orientation angles. From this study it is shown that when the orientation angle

of the interconnections is zero degrees then a strong interface is formed. Furthermore the application of the variable peel angle in the peeling process ensures the requirement of comparatively lesser de-bonding force for self-detachment of the parallel nanotube bundles from their forest. Thus, the initiation and continuous production of spinnable carbon nanotube web in macro scale is possible. Hence, the influence of peeling mechanics in the manufacturing process and mechanical performances of macro scale carbon nanotube items is revealed in this study.

References

- [1] Davis WR, Slawson RJ, Rigby GR. An unusual form of carbon. *Nature* 1953;171(4356):756.
- [2] Hofer LJE, Sterling E, McCartney JT. Structure of carbon deposited from carbon monoxide on iron, cobalt and nickel. *J Phys Chem* 1955;59(11):1153–5.
- [3] Iijima Sumio, Ichihashi Toshinari. Single-shell carbon nanotubes of 1-nm diameter. *Nature* 1993;363(6430):603–5.
- [4] Kuznetsov Alexander A, Fonseca Alexandre F, Baughman Ray H, Zakhidov Anvar A. Structural model for dry-drawing of sheets and yarns from carbon nanotube forests. *ACS Nano* 2011;5:985–93.
- [5] Khandoker N, Hawkins SC, Ibrahim R, Huynh CP, Deng F. Tensile strength of spinnable multiwall carbon nanotubes. *Proc Eng* 2011;10:2572–8.
- [6] Cumings John, Zettl A. Low-friction nanoscale linear bearing realized from multiwall carbon nanotubes. *Science* 2000;289:602–4.
- [7] Wei Xiaoding, Naraghi Mohammad, Espinosa Horacio D. Optimal length scales emerging from shear load transfer in natural materials: application to carbon-based nanocomposite design. *ACS Nano* 2012;6(3):2333–44.
- [8] Pogorelov Evgeny G, Zhanov Alexander I, Chang Yia-Chung, Yang Sung. Universal curves for the van der Waals interaction between single-walled carbon nanotubes. *Langmuir* 2012;28:1276–82.
- [9] Sun Zuo, Dillard David A. Three-dimensional finite element analysis of fracture modes for the pull-off test of a thin film from a stiff substrate. *Thin Solid Films* 2010;518:3837–43.
- [10] Ostrowicki GT, Sitaraman SK. Magnetically actuated peel test for thin films. *Thin Solid Films* 2012;520:3987–93.
- [11] Spies GJ. The peeling test on redux bonded joints. *J Aircraft Eng* 1953;25:64–70.
- [12] Kendall K. Thin-film peeling – the elastic term. *J Phys D Appl Phys* 1975;8:1449–52.
- [13] Bikerman JJ. Theory of peeling in hookean solid. *J Appl Phys* 1957;28(12):1484–5.
- [14] Kim KS, Aravas N. Elastoplastic analysis of the peel test. *Int J Solids Struct* 1988;24(4):417–35.
- [15] Gent AN, Hamed GR. Peel mechanics. *J Adhes* 1975;7:91–5.
- [16] Kinloch AJ, Lau CC, Williams JG. The peeling of flexible laminates. *Int J Fract* 1994;66:45–70.
- [17] Williams JG. Energy release rate for the peeling of flexible membranes and the analysis of blister tests. *Int J Fract* 1997;87:265–88.
- [18] Thouless MD, Jensen HM. Elastic fracture mechanics of the peel-test geometry. *J Adhes* 1992;38(3–4):185–97.
- [19] Suo Z, Hutchinson JW. Interface crack between two elastic layers. *Int J Fract* 1990;43:1–18.
- [20] Thouless MD, Yang QD. A parametric study of the peel test. *Int J Adhes Adhes* 2008;28:176–84.
- [21] Huynh Chi P, Hawkins Stephen C. Understanding the synthesis of directly spinnable carbon nanotube forests. *Carbon* 2010;48:1105–15.
- [22] Huynh Chi P, Hawkins Stephen C, Redrado Marta, Barnes Scott, Lau Deborah, Humphries William, et al. Evolution of directly-spinnable carbon nanotube growth by recycling analysis. *Carbon* 2011;49:1989–97.
- [23] Zhang Mei, Fang Shaoli, Zakhidov Anvar A, Lee Sergey B, Aliev Ali E, Williams Christopher D, et al. Strong, transparent, multifunctional, carbon nanotube sheets. *Science* 2005;309(5738):1215–9.
- [24] Kelly BT. Physics of graphite. London: Applied Science; 1981.
- [25] Jia Yuanyuan, Yan Wenyi, Liu Hong-Yuan. Carbon fibre pullout under the influence of residual thermal stresses in polymer matrix composites. *Comput Mater Sci* 2012;62:79–86.
- [26] Williams JG, Hadaviniad H, Cotterell B. Anisotropic elastic and elastic-plastic bending solutions for edge constrained beams. *Int J Solids Struct* 2005;42:4927–46.
- [27] Israelachvili Jacob N. Intermolecular and surface forces. 3rd ed. Elsevier; 2011.
- [28] Argento C, Jagota A, Carter WC. Surface formulation for molecular interactions of macroscopic bodies. *J Mech Phys Solids* 1997;45(7):1161–83.
- [29] De Lorenzis Laura, Zavarise Giorgio. Modeling of mixed-mode debonding in the peel test applied to superficial reinforcements. *Int J Solids Struct* 2008;45(20):5419–36.
- [30] Khandoker Noman, Hawkins Stephen C, Ibrahim Raafat, Huynh Chi P. Peel test of spinnable carbon nanotube webs. *Physica E* 2014;60:160–5.
- [31] Elambasseril J, Ibrahim RN. Determination of interfacial fracture toughness of coatings using circumferentially notched cylindrical substrate. *Mater Sci Eng A* 2011;529:406–16.
- [32] Elambasseril J, Ibrahim RN. Quantitative evaluation of the adhesion of metallic coatings using cylindrical substrate. *Mater Des* 2012;33:641–51.